Structural analysis of sulfate vein networks in Gale crater (Mars)

Barbara de Toffoli, Nicolas Mangold, Matteo Massironi, Alain Zanella, Riccardo Pozzobon, Stéphane Le Mouélic, Jonas L'Haridon, Gabriele Cremonese

STRUCTURAL ANALYSIS OF SULFATE VEIN NETWORKS IN GALE CRATER (MARS)

Barbara De Toffoli [a,b,d*], Nicolas Mangold [b], Matteo Massironi [a,d], Alain Zanella [c]

Riccardo Pozzobon [a,d], Stephane Le Mouélic [b], Jonas L'Haridon [b], Gabriele Cremonese [d]

[a] Department of Geosciences, University of Padova, Via Gradenigo 6, Padova 35131, Italy

[b] Laboratoire de Planetologie et Geodynamique, Universite de Nantes, CNRS UMR 6112, Nantes, France

[c] Department of Geology, Université du Maine, Le Mans, France

[d] INAF, Osservatorio Astronomico di Padova, Vicolo dell'Osservatorio 3, Padova I-35122, Italy

* Corresponding author: tel. +39 3772678273, email: barbara.detoffoli@unipd.it & barbara.detoffoli@gmail.com

Abstract

The Curiosity rover's campaign in the Gale crater on Mars provides a large set of close-up images of sedimentary formations outcrops displaying a variety of diagenetic features such as light-toned veins, nodules and raised ridges. Through 2D and 3D analyses of Mastcam images we herein reconstruct the vein network of a sample area and estimated the stress field. Assessment of the spatial distribution of light-toned veins shows that the basin infillings, after burial and consolidation, experienced a sub-vertical compression and lateral extension coupled with fluid overpressure and cracking. Overall, rock failure and light-toned veins formations could have been generated by an overload produced by a pulse of infilling material within the basin.

Keywords: Mars – veins – fluid circulation – Curiosity rover – hydrofracturing

1. Introduction

NASA's Mars Science Laboratory mission, Curiosity, has been surveying the Gale crater since August 2012. It is equipped with a set of 17 cameras and 10 scientific instruments that allow rock and soil sample observation and analysis. Thanks to the *in situ* observations of the rover it has been possible to recognize fluid circulation features emplaced during diagenesis subsequent to burial and consolidation of the sediments. Specifically cross-cutting light-toned veins (Grotzinger et al., 2014, L'Haridon et al., 2018; Nachon et al., 2014, 2017), nodules (Stack et al., 2014) and raised ridges (Siebach et al., 2014; Léveillé et al., 2014; McLennan et al., 2014) were detected. According to ChemCam's Laser Induced Breakdown Spectroscopy (LIBS) measurements, the light-toned veins have a Ca-sulfate mineralogy (Nachon et al., 2014) mainly interpreted to be bassanite ($CaSO_4 \times 0.5\ H_2O$) at least on the surface exposed portions of the investigated outcrops (Rapin et al., 2016). These veins are observed throughout most of the outcrops recorded on the Curiosity traverse, especially in the fine-grained sandstones and mudstones, interpreted to be fluvial and lacustrine in origin (Grotzinger et al., 2014, 2015). The genesis of the veins is suggested to be ascribable to fluid flows that led to dissolution and re-precipitation of sulfate-rich materials (L'Haridon et al., 2018; Vaniman et al., 2018; Rapin et al., 2016; Schwenzer et al., 2016, Caswell and Milliken, 2017). Veins with mineral infilling are associated to two main stages of formation: i) the generation of fractures, which is a consequence of stresses and/or fluid overpressure produced by several factors such as fluid thermal expansion, the generation of fluid (i.e. diagenetic fluid expulsion), or chemical compaction; ii) the mineral infilling, which implies mineral dissolution, transport and precipitation that may occur to form single or multiple veins (e.g. Bjørlykke, 1997; Philipp, 2008). Thus fluids, a material source (with suitable T and P conditions for precipitation) and fractures providing space for precipitation are the key ingredients to produce a network of mineral veins such as the ones observed at Gale crater.

49 The purpose of this study is to assess the structural behaviour recorded by a well-exposed
50 crack system in a case study area along the rover traverse, to reconstruct the fracturing
51 mechanisms, deduce the pattern of stress during fluid circulation and therefore provide some
52 insights on the origin of the regional deformation involved during the formation of these features.

53 **2. Geological Background**

54 Gale is a complex crater located on the border of highlands close to the Martian dichotomy
55 (5.37°S, 137.81°W) and filled by sedimentary deposits forming a central mound, Aeolis Mons
56 (informally known as Mount Sharp). Gale crater is around 150 km in diameter and displays ~5 km
57 of elevation difference between the floor and the central peak and rims (Young and Chan, 2017;
58 Stack et al., 2016; Grotzinger et al., 2014, 2015; Le Deit et al., 2013; Wray, 2012). The meteor
59 impact that formed Gale crater has been estimated to have occurred around the Noachian-
60 Hesperian boundary (e.g. Le Deit et al., 2013; Thomson et al., 2011; Irwin et al., 2005). In the Late
61 Noachian/Early Hesperian epoch a major climatic change led water to be increasingly unstable at
62 surface conditions that Gale crater experienced and recorded. In fact, Gale crater has experienced
63 an intricate evolution involving the past presence of surface water indicated by rim-crossing carved
64 channels and lacustrine deposits at the mound base (e.g. Le Deit et al., 2013, Palucis et al., 2014,
65 Grotzinger et al., 2014; Thomson et al., 2011; Milliken et al., 2010), this site is invaluable for the
66 paleoenvironment reconstruction and pivotal for the investigation of Martian habitability (e.g.
67 Rubin et al., 2017, Caswell and Milliken, 2017).

68 Three main sedimentary groups have been identified in-situ by Curiosity rover investigations:
69 the Bradbury group, the Mount Sharp group and the Siccar Point group (Fig.1; Grotzinger et al.,
70 2014, 2015; Treiman et al., 2016). The first two groups are representative of a fluvio-lacustrine
71 environment recorded by laminated and cross stratified mudstones, sandstones and pebble
72 conglomerates, recognized especially at Pahrump Hills which is part of the Murray formation of
73 Mount Sharp group (e.g. Le Deit et al., 2016; Treiman et al., 2016; Stack et al., 2015; Bristow et

al., 2015; Grotzinger et al., 2014, 2015). The third group is dominated by eolian sedimentary rocks that were accumulated unconformably over the other two and cemented (Banham et al., 2018).

Light-toned veins have been observed pervasively inside the Bradbury and Mount Sharp group at a varying frequency (Watkins et al., 2017, L'Haridon et al., 2018). Some veins cross the unconformity with the overlying eolian sedimentary rocks from the Siccar Point group (e.g. Frydenvang et al., 2017) showing that some of them formed well-after the cementation and erosion of the sedimentary layers. A remarkable part of the collected evidence related to the light-toned veins are based on the compositional information acquired with ChemCam (Maurice et al., 2012; Wiens et al., 2012) and its synergy with other instrument suites onboard Curiosity (e.g. CheMin, Chemical and Mineralogy, and MAHLI, Mars Hand Lens Imager). The light-toned veins have a calcium and sulfur-rich chemistry consistent with a Ca-sulfate mineralogy (Nachon et al., 2014), mainly interpreted to be bassanite from the analysis of the hydrogen emission line (Rapin et al., 2016).

The sedimentary rocks of interest for our work are located in the Murray formation, which is at the base of the Mount Sharp group. The Murray formation is composed of mudstones predominantly, with local fine-grained sandstones (Stein et al., 2018). An enhanced chemical alteration has been suggested from the presence of a large fraction of phyllosilicates (up to 25% in volume) and high values of chemical indices of alteration (Bristow et al., 2018, Mangold et al., 2019). The Murray mudstones have been affected by a widespread post-depositional history as observed through features such as fracture fills, veins, ridges and nodules, all indicating a complex diagenetic history, not limited to the light-toned veins focused in our study (Grotzinger et al., 2015, Nachon et al., 2017, L'Haridon et al., 2018). Investigating possible source of fluids that interplayed in fractures development would lead to a better understanding of the sulfate veins' origins (e.g. Schwenzer et al., 2016; Grotzinger et al., 2014, 2015, L'Haridon et al., 2018, Gasda et al., 2018). Sources of sulfates have been suggested to be localized on higher (Nachon et al., 2017), lower (Grotzinger et al., 2014; McLennan et al., 2014; Nachon et al., 2017) or lateral (McLennan et al.,

2014) layers with the respect of the fractured ones, whose fluid content underwent mobilization during a late diagenetic event (Nachon et al., 2017; Young and Chan, 2017 and references therein). Because of the ubiquitous presence of veins, a recent study proposed a paleoenvironmental evolution at the entire basin scale that could lead to deposition, accumulation, burial, dissolution and reprecipitation of the sulfates that filled the light-toned veins of Gale (Schwenzer et al., 2016). The light-toned veins of the Gale Crater seem to be similar to those observed in many sedimentary basins on Earth. This is especially the case for bedding-parallel fibrous gypsum veins called 'beef' veins (Buckland & De La Bèche, 1835) or 'BPV' for Bedding-parallel veins (e.g. Ukar et al., 2017). Several recent worldwide reviews demonstrate that these mineralized veins are very widespread on Earth, especially within impermeable and anisotropic materials such as mudstones (Cobbold et al., 2013; Gale et al., 2014). These veins are interpreted to be the result of fluid-assisted fracturing due to pore fluid overpressures and stresses (e.g. Cobbold & Rodrigues, 2007; Cobbold et al., 2013)

We collected structural data based on the distribution of light-toned veins distinguishable in the area that the Curiosity rover observed between sol (Martian days)1536 and 1545 (Fig.1a). While many outcrops of the Murray formation were either flat or partly buried below sand, this location was chosen because of the presence of clean blocks, less than 1 m high, where light-toned veins are visible enabling a detailed structural analysis using image analysis and photogrammetry helped by the large number of image available.

3. 3D reconstruction and measurements

To investigate the light-toned veins that have been detected in Gale crater we performed 2D and 3D analyses of Mastcam and Navcam Curiosity images. Mastcam takes colour images of 1600 × 1200 pixels that can be stitched together to create panoramas of the landscape around the rover.

Mastcam consists of a two-camera system that can acquire true RGB colour images, using a Bayer filter, approximating what human eyes would perceive on Mars (Bell et al., 2012). With respect of the scientific purpose of Mastcam, the Navcam camera pairs were planned for operational use including acquisition of images for the rover's navigation, robotic planning and documentation, remote sensing science instrument pointing, but also general surface imaging (Maki et al., 2011). We coupled 2D mosaics of Mastcam images and the production of a 3D Digital Outcrop Model (DOM) (e.g. Caravaca et al., 2019) of the same region from both Mastcam and Navcam in order to reconstruct the fracture distribution in the area of interest which covers ~100 m^2 (Fig.2).

2D images were observed raw and stitched together, where overlapping acquisitions of neighbouring areas were available, in order to exploit full resolution image data for the detection of fractures' characterizing marks (e.g. junctions and lateral continuity) and local distributions in relation to other fracture sets and sediment laminations. We performed 3D reconstruction of the same investigated outcrops by means of the Agisoft software (Wagner et al., 2014) from multiple images taken by Mastcam binocular stereo vision and Navcam systems. Agisoft PhotoScan (recently renamed Metashape) is a 3D advanced modelling package based on image data processing which can automatically build the models without setting initial values and control points. It processes images taken at any position and angle as far adjacent photos share corresponding points recognizable on the targets. The scale computed by the software was tested by comparing it with known size objects such as rovers' wheels. Loading the images into Agisoft, the software automatically searches for the corresponding points matching and aligning the photos and finally generating a sparse point cloud. When the automatic alignment procedure failed, tie points were manually implemented in the system to exploit the maximum number of images available. On the point cloud, that is generally denser closer to the observation point and favourably oriented surfaces, an irregular triangle net can be built, then the texture mapping is carried out according to the produced triangle net. We carried out the further step of elaboration by using the Cloud Compare environment, which is a 3D point cloud and triangular mesh

processing software that allows the user to interact with 3D entities rotating, translating, drawing 2D polylines, picking points and extracting correspondent 2D and 3D information. In this context veins were marked by tracing polylines and further structural information (i.e. dip direction and dip angle, intersections angles, kinematics estimates) was developed by plane fitting and contextual data extraction through the Cloud Compare compass plugin.

4. Results

Both from 2D images and 3D reconstruction, the presence of different sets of non-randomly distributed fractures was neatly recognizable. All the fractures appear to have a higher resistance against erosion with respect of the host rock, in fact they tend to stick out from the knobs leading to an easy identification all over the outcrops. The first general distinction is the overall presence of one population of bedding-parallel light-toned veins and a second population of middle to high-angle dipping light-toned veins (Fig.3).

Bedding-parallel veins do not show significant thickness variations (averagely <1 cm) both at the single vein scale and among the general population, although lateral continuity is unclear and visible edges appear rounded and jagged, thus a patched distribution seems to be overall the most reasonable. Bedding-parallel veins show a well recognizable undulate, slightly wandering trend as recognizable in the measurements which display an averagely 15° dipping angle variation range and a broad variability among the recorded dip directions (Fig.4g) due to the variability of the available data, i.e. the outcropping visible veins, randomly sampling the undulate trend. Despite a consistently average horizontal sub-parallel behaviour at the scale of the study area, bedding-parallel veins show in places a cross cutting relationship bending and stopping on the neighbouring ones (Fig.3b).

Oblique veins appear less frequent than the sub-horizontal population. These veins display clear “en-echelon” structures well recognizable by the distinctive arrays of sigmoidal shaped

177 cracks (Nicholson and Pollard, 1985) that propagate from the margin of a larger parent crack,
178 twisting out and bending as the result of mechanical interaction between tips of adjacent parallel
179 cracks (Pollard et al. 1982). Such geometries are used to infer the state of deformation (Ramsay &
180 Huber 1983) or the state of stress (Pollard et al. 1982, Rickard & Rixon 1983) in the surrounding
181 rock at the time of cracking and accordingly, in the specificity of this case study, the "en-echelon"
182 features display an extensional component. We measured two different sets of oblique cracks
183 based on dip/dip-direction trends: (i) one with an average value of dip direction: 290°N and dip:
184 67° (spanning between minimum and maximum values of: 264°-309° dip direction and 54°-77°
185 dip) and a (ii) second one showing a dip direction-dip average value of 155°N - 53° (spanning
186 between minimum and maximum values of: 126°-184° dip direction and 31°-71° dip). On a
187 vertical section (as the ones provided by the outcrops walls facing toward the Curiosity rover), the
188 two populations of oblique fractures are thus intersecting at an average angle of 60° according to
189 the measurements, as illustrated by single outcrops where fractures from both the oblique sets are
190 visible (Fig.3).
191 In the study area it was also possible to observe cross-cutting relationships between the
192 different sets above distinguished by orientation. No evidence of displacement was found and
193 neither recurrent truncation of one set on the other were observed to determine an occurrence
194 sequence (Fig.3c).

195

196 **5. Discussions**

197

198 On Mars, the combination of 2D and 3D products on the Gale crater floor with high-resolution
199 in situ data along the rover track allows to pursue a structural interpretation of the basin at the time
200 of the generation of the light-toned veins. The general trend of all the plain sets to crosscut the host
201 rock laminations leads in first place to exclude a depositional layering interpretation. The presence

of two cross-cutting sets of light-toned vein sets arranged ~60° apart and displaying en-echelon structures highlighting shear sense that led to a lowering of the hanging wall suggest an, at least partial, regime of extension. Accordingly, the maximum principal stress is suggested to bisect the acute angle occurring between the sets that in the specificity of this case would mean that σ1 lays on a sub-vertical axis. The minimum σ3 orientation accordingly lays on a sub-horizontal plane and displays NW-SE direction (Fig.4).

The set of horizontal veins is well-matching disposition and morphology of failures induced by fluid overpressure recorded on Earth that happened during the fluid resurgence cracking the host rock along fresh planes or exploiting previously existing surfaces of weakness such as the mudstone bedding and laminations.

An example of the formation process that produced the horizontal vein set is the paleo-hydrofracturing model of gypsum veins in the lower Mercia Mudstone Group (Philipp, 2008). This group outcrops on the Somerset Coast of SW England, Watchet Bay, and display analogue characteristics to the rocks observed in the Gale crater (e.g. Young and Chan, 2017; Cobbold et al., 2013). The lower part of the Mercia Mudstone Group consists of several tens of meters of poorly bedded, red to reddish-brown unfossiliferous mudstones and siltstones (Whittaker and Green, 1983; Leslie et al., 1993), whereas in the upper part the red mudstones are characterized by laterally discontinuous evaporite-rich horizons, mainly composed of white nodular gypsum (Philipp, 2008). In the Mercia Mudstone Group vein dips show variations from horizontal to vertical and the strikes are in broad range of directions, no clear predominant attitude was detected. Crosscutting relationships were investigated as well and indicated no prevalent age relationship suggesting that the veins may all have formed at the same time (Philipp, 2008). The formation is interpreted to have formed in a playa lake or desert plain conditions (Bennison & Wright, 1969; Simms & Ruffell, 1990), where ephemeral pools were likely to be present and remobilization and accumulation of gypsum primarily disseminated in the sediment could have happened (Leslie et al., 1993). In Watchet Bay fluid transport took place mainly along faults and fractures since

mudstones have a very low original permeability and are commonly effective barriers to fluid circulation (Philipp, 2008; Cartwright, 1997). The outcrops show discontinuous anastomosing networks of gypsum veins confined to portions of the hosting mudstone. The phenomenon is not pervasive to the whole mudstone group though, but it is confined to specific portions often overlain by thick grey siltstone layers weakly calcareous (Philipp, 2008). It may in fact occur that veins produced by hydrofracturing stop where mechanical contrast boundaries occur (e.g. Brenner and Gudmundsson, 2004b; Gudmundsson et al., 2002; Cosgrove, 2001; Gudmundsson and Brenner, 2001). There is no need of active slipping faults to allow fluid circulation and hydrofracturing, that are triggered when the pressure of the fluids sited within the veins exceed the lithostatic pressure (Ramsey, 1980). When fluids are involved (e.g. geothermal fluids), buoyancy overpressure can convey a significant contribution to the fracturing process. Depending on the stress field, fluids can be transported along the veins (i) leading to hydrofracturing propagation of already existing fracture plains and anisotropies (i.e. bedding plains and laminations) or (ii) generating hydrofracturing into the host rock (Philipp, 2008 and references therein). Philipp (2008) suggests an hydrofracturing model to explain the sulphate vein network systems that cut the Mercia Mudstone Group based on low permeability of the mudstone that drove fluids, flowing from the highest to the lowest hydraulic potential (Domenico & Schwartz, 1998), to enter the rocks along faults and fractures and prevented them to penetrate intimately the host rock.

The fluid source for the Martian case study is not entirely clear; fluid flow can be triggered by very diverse physical and chemical disequilibria that might generate fluid overpressure. Some examples could be compaction due to burial, diagenetic fluid expulsion and buoyancy, crystallization, porosity changes and thermal expansion (Neuzil, 1995; Bjørlykke, 1997; Osborne & Swarbrick, 1997). On Mars, Gale experienced water-rich early stages (Late Noachian/Early Hesperian) during which the crater could have been connected to both surficial and underground water reservoirs (e.g., Villanueva et al. 2015; Andrews-Hanna et al., 2010), thus implying

253 potentially transient flooding and drying in sabkha or ephemeral lake environments leading to
254 mineral (e.g. salts) precipitation and accumulation in the basin (Rapin et al., 2019).

255 Nevertheless, these veins are not likely to have formed early in the basin history, but when
256 compaction, consolidation and diagenetic processes started affecting the region. In fact a
257 significant part of the vein population consists of well recognisable fractures cross-cutting rock
258 bedding, hence the mudstone must have had some shear strength at the time of formation to trigger
259 a brittle response thus excluding a young soft host rocks (Schwenzer et al., 2016; Philipp, 2008;
260 Bell, 2000). Thus, subsequent dissolution and mobilization by diagenetic fluids of initial deposits,
261 of unclear stratigraphic position yet, may have led to the formation of the sulphate veins observed
262 on the rover traverse (L'Haridon et al., 2018; Schwenzer et al., 2016; Nachon et al., 2017;
263 Grotzinger et al., 2014; McLennan et al., 2014).

264

265 **6. Conclusions**

266

267 Light-toned fracture networks have been observed repeatedly along Curiosity rover traverse
268 (e.g. Watkins et al., 2017) and their distribution reflects the stress field they have been exposed to
269 at the moment of fracturing. Within the window of ten sols (sol 1536 – sol 1545) herein analysed,
270 Curiosity acquired a large number of images from different angles of a field of bedrock knobs
271 cropping out from the sand where many sulphate veins were neatly visible. This asset allowed the
272 3D reconstruction of the area and, contextually, the 3D reconstruction of the plane set where
273 fractures lay. On Earth, similar arrangements can be observed at Watchet Bay where networks of
274 intersecting sulphate veins developed thanks to hydrofracturing regimes within reddish mudstone
275 levels.

276 In Gale, the fracturing process is therefore to be ascribed to two different complementary
277 contributions: (i) the 60° dipping fractures are to be considered the product of an extensional
278 regime where the principal stress lays on a vertical axis (Fig.3a); (ii) the set of bedding-parallel

fractures are the result of a hydrofracturing process where fluid overpressure was energetic enough to open new fractures just in places, but mostly used pre-existing weakness surfaces constituted by mudstone layering. Additionally, the formation of the bedding-parallel vein set might have been synchronous to the formation of the other two sets since no truncation or displacement have been observed around the available outcrops. This interpretation is well supported by the geological context. Gale is a large crater that experienced water and sediment infilling, the vertical maximum stress is reasonably to be ascribed to such progressive overload. The cracking drive of hydrofracturing, can be triggered either by the emplacement of an overburden that perturbs fluid pressure, or as response to an unloading event when pressurized fluids are already stored in the subsurface. The origin of fluids at Gale is still debated and overpressure cracking itself does not carry enough information to discriminate it. In the hypothesis of a coeval genesis of the oblique and the bedding-parallel vein networks, a pulse of material overload within the crater could have been responsible both for the extensional failure and the fluid escape from the already consolidated deposits on the crater floor. In this context, due to the crater circular shape, maximum extension is accordingly expected to develop along the radial directions. This is confirmed by σ3 NE-SW direction recorded in the study area, σ3 thus locally appears to develop radially compared to the closest crater rim. However, to better constrain the scenario, it would be necessary to collect data from multiple sites along the rover traverse in order to check the behaviour of σ3 at different position with the respect of the crater rim.

Veins mapping and reconstruction allowed the production of a well constrained structural context interpretation and cracking driving forces identification which are likely to have been active in the whole crater area so producing a structural context for the entirety of the fracture and vein networks that have been recorded along the rover traverse.

Acknowledgments

This paper is part of a project supported by the European Union's Horizon 2020 research and innovation program under grant agreement Nº776276 (PLANMAP) and has been supported by the "Fondazione Ing. Aldo Gini" scholarship. Some of the authors were funded by the Centre National d'Etudes Spatiales (CNES). The data reported in this paper are archived at the Planetary Data System, accessible at http://pds-geosciences.wustl.edu/missions/msl/index.htm. We are indebted to the Mars Science Laboratory Project engineering and science teams for their diligent efforts in making the mission as effective as possible and for their participations in tactical and strategic operations.

References

Andrews-Hanna, J.C., et al., 2010. Early Mars hydrology: Meridiani playa deposits and the sedimentary record of Arabia Terra. J. Geophys. Res. E Planets 115, 1–22. https://doi.org/10.1029/2009JE003485

Banham, S. G. et al. (2018) Ancient Martian aeolian processes and palaeomorphology reconstructed from the Stimson formaton on the lower slope of aeolis Mons, Gale Crater, Mars, Sedimentology, 65, 993-1042.

Bell, F. G., 2000. Engineering Properties of Soils and Rocks. Oxford: Blackwell.

Bell, J. F., et al., 2012. Mastcam multispectral imaging on the Mars Science Laboratory rover: wavelength coverage and imaging strategies at the gale crater field site, Lunar Plan. Sci. Conference, pp 2541

Bennison, G. M. and Wright, A. E. 1969. The Geological History of the British Isles. London: Edward Arnold Ltd, 406 pp.

Bjørlykke, K. 1997. Lithological control on fluid flow in sedimentary basins. In Fluid Flow and Transport in Rocks (eds B. Jamtveit & B. W. D. Yardley), pp. 15– 34. London: Chapman and Hall.

Brenner, S. L. & Gudmundsson, A. 2004b. Arrest and aperture variation of hydrofractures in layered reservoirs. In The Initiation, Propagation and Arrest of Joints and Other Fractures (eds J. W. Cosgrove & T. Engelder), pp. 117–28. Geological Society of London, Special Publication no. 231.

Bristow, T. F., et al., 2015. The origin and implications of clay minerals from Yellowknife Bay, Gale crater, Mars, Am. Mineral., 100, 824–836, doi:10.2138/am-2015-5077CCBYNCND.

Buckland and De la Beche, 1835. On the Geology of the Neighbourhood of Weymouth and the Adjacent Parts of the Coast of Dorset Transactions of the Geological Society, London 2–4, pp. 1–46

Caravaca, G.; Le Mouélic, S.; Mangold, N.; L'Haridon, J.; Le Deit, L.; Massé, M., 2019. 3D Digital Reconstruction of the Kimberley Outcrop (Gale Crater, Mars) from Photogrammetry Using Multi-Scale Imagery from Mars Science Laboratory 50th Lunar and Planetary Science Conference

Cartwright, J. A. 1997. Polygonal extensional fault systems: a new class of structure formed during the early compaction of shales. In Fluid Flow and Transport in Rocks (eds B. Jamtveit & B. W. D. Yardley), pp. 35–56. London: Chapman & Hall.

Caswell, T.E., Milliken, R.E., 2017. Evidence for hydraulic fracturing at Gale crater, Mars: implications for burial depth of the Yellowknife Bay formation. Earth Planet. Sci. Lett. 468, 72–84. doi:10.1016/j.epsl.2017.03.033.

Cobbold, P.R., Zanella, A., Rodrigues, N., Løseth, H., 2013. Bedding-parallel fibrous veins (beef and cone-in-cone): worldwide occurrence and possible significance in terms of fluid overpressure, hydrocarbon generation and mineralization, Mar. Pet. Geol., 43, pp. 1-20, 10.1016/j.marpetgeo.2013.01.010

Cobbold, P.R., Rodrigues, N., 2007. Seepage forces, important factors in the formation of horizontal hydraulic fractures and bedding-parallel fibrous veins ("beef" and "cone-in-cone"), Geofluids, 7, pp. 313-322, 10.1111/j.1468-8123.2007.00183.x

Cosgrove, J.W., 2001. Hydraulic fracturing during the formation and deformation of a basin: A factor in the dewatering of low-permeability sediments. Am. Assoc. Pet. Geol. Bull. 85, 737–748. https://doi.org/10.1306/8626C997-173B-11D7-8645000102C1865D

Domenico, P. A. & Schwartz, F. W. 1998. Physical and Chemical Hydrogeology, 2nd ed. New York: Wiley, 506

Frydenvang J. et al., 2017. Diagenetic silica enrichment and late-stage groundwater activity in Gale crater, Mars. Geophys. Res. Let., 44, 4716-4724.

Gale, J.F.W., Laubach, S.E., Olson, J.E., Eichhubl, P., FallA., 2014. Natural fractures in shale: A review and new observations, AAPG Bulletin, 98 (11): 2165–2216. doi: https://doi.org/10.1306/08121413151

Gasda, P. J., et al. (2017) In situ detection of boron by ChemCam on Mars, Geophysical Research Letters, 44, 8739-8748.

Grotzinger, J.P., et al., 2014. A habitable fluvio-lacustrine environment at Yellowknife Bay, Gale crater, Mars. Science (80–) 343 (6169). 1242777–1242777 doi: 10.1126/ science.1242777.

Grotzinger, J.P., et al., 2015. Deposition, exhumation, and paleoclimate of an ancient lake deposit, Gale crater, Mars. Science (80–) 350 (6257). aac7575-aac7575 doi: 10.1126/science.aac7575.

Gudmundsson, A. & Brenner, S. L. 2001. How hydrofractures become arrested. Terra Nova 13, 456–62.

Gudmundsson, A., et al., 2002. Propagation pathways and fluid transport of hydrofractures in jointed and layered rocks in geothermal fields. Journal of Volcanology and Geothermal Research 116, 257–78.

364 Hurowitz, J.A., Grotzinger, J.P., Fischer, W.W., McLennan, S.M., Milliken, R.E., Stein, N., Vasavada, A.R.,
365 Blake, D.F., Dehouck, E., Eigenbrode, J.L., Fairén, A.G., Frydenvang, J., Gellert, R., Grant, J.A., Gupta, S.,
366 Herkenhoff, K.E., Ming, D.W., Rampe, E.B., Schmidt, M.E., Siebach, K.L., Stack-Morgan, K., Sumner,
367 D.Y., Wiens, R.C., 2017. Redox stratification of an ancient lake in Gale crater, Mars. Science (80-.). 356.
368 https://doi.org/10.1126/science.aah6849
369 Irwin, R. P., A. D. Howard, R. A. Craddock, and J. M. Moore (2005), An in- tense terminal epoch of widespread
370 fluvial activity on early Mars: 2. Increased runoff and paleolake development, J. Geophys. Res., 110,
371 E12S15, doi:10.1029/2005JE002460.
372 L'Haridon, J., Mangold, N., Meslin, P.-Y., Johnson, J. R., Rapin, W., Forni, O., et al. (2018). Chemical variability
373 in mineralized veins observed by ChemCam on the lower slopes of Mount Sharp in Gale crater, Mars. Icarus,
374 311, 69–86. https://doi.org/10.1016/j.icarus.2018.01.028
375 Le Deit, L., E. Hauber, F. Fueten, M. Pondrelli, A. P. Rossi, and R. Jaumann (2013), Sequence of infilling events in
376 Gale Crater, Mars: Results from morphology, stratigraphy, and mineralogy, J. Geophys. Res. Planets, 118,
377 doi:10.1002/ 2012JE004322.
378 Le Deit, L., et al., 2016. The potassic sedimentary rocks in Gale crater, Mars, as seen by ChemCam on board
379 Curiosity. J. Geophys. Res. Planets 121 (5), 784–804. doi:10.1002/2015JE004987.
380 Leslie, A. B., et al., 1993. Geochemical and mineralogical variations in the upper Mercia Mudstone Group (Late
381 Triassic), southwest Britain: correlation of outcrop sequences with borehole geophysical logs. Journal of the
382 Geological Society, London 150, 67–75.
383 Léveillé, R.J., et al., 2014. Chemistry of fracture-filling raised ridges in Yellowknife Bay, Gale crater: window into
384 past aqueous activity and habitability on Mars. J. Geophys. Res. Planets 119 (11), 2398–2415.
385 doi:10.1002/2014JE004620.
386 Maki, J. N., et al., 2011. The Mars Science Laboratory (Msl) Navigation Cameras (Navcams), Lunar Plan. Sci.
387 Conference, pp 2738
388 Mangold, N., Dehouck, E., Fedo, C., Forni, O., Achilles, C., Bristow, T., Downs, R.T., Frydenvang, J., Gasnault,
389 O., L'Haridon, J., Le Deit, L., Maurice, S., McLennan, S.M., Meslin, P.Y., Morrison, S., Newsom, H.E.,
390 Rampe, E., Rapin, W., Rivera-Hernandez, F., Salvatore, M., 2019. Chemical alteration of fine-grained
391 sedimentary rocks at Gale crater. Icarus 321, 619–631.
392 Maurice, S. and 69 co-authors, 2012. The ChemCam instrument suite on the Mars Science Laboratory (MSL)
393 rover: Science objectives and mast unit description. Space Sci. Rev., 170 :95-166, doi 10.1007/s11214-012-
394 9912-2.

McLennan, S.M., et al., 2014. Elemental geochemistry of sedimentary rocks at Yel- lowknife Bay, Gale crater, Mars. Science (80–) 343 (6169), 1244734. doi:10.1126/ science.1244734.

Milliken, R.E., et al., 2010. Paleoclimate of Mars as captured by the stratigraphic record in Gale crater. Geophys. Res. Lett. 37 (4), 1–6. doi:10.1029/2009GL041870.

Nachon, M., et al., 2014. Calcium sulfate veins characterized by ChemCam/Curiosity at Gale crater, Mars. J. Geophys. Res. Planets 119 (9), 1991–2016. doi:10.1002/ 2013JE004588.

Nachon, M., et al., 2017. Chemistry of diagenetic features analyzed by ChemCam at Pahrump Hills, Gale crater, Mars. Icarus 281, 121–136. doi:10.1016/j.icarus.2016.08. 026.

Neuzil, C. E. 1995. Abnormal pressures as hydrodynamic phenomena. American Journal of Science 295, 742–86.

Nicholson, R. & Pollard, D.D. 1985. Dilation and linkage of en-echeleon cracks. Journal of Structural Geology, 7, 583–590.

Osborne, M. J. & Swarbrick, R. E. 1997. Mechanisms for generating overpressure in sedimentary basins: A reevaluation. American Association of Petroleum Geologists Bulletin 81, 1023–41.

Palucis, M., W. Dietrich, A. Hayes, R. Williams, S. Gupta, N. Mangold, H. E. Newsom, C. Hardgrove, F. Calef, D. Sumner, 2014, The origin and evolution of the Peace Vallis fan system that drains to the Curiosity landing area, Gale Crater, Mars, J. Geophys. Res. Planets, 119, 705–728, doi:10.1002/2013JE004583

Phillip, S. L., 2008. Geometry and formation of gypsum veins in mudstones at Watchet, Somerset, SW England, Geol. Mag., 145(6), 831–844, doi:10.1017/S0016756808005451.

Pollard, D. D., Segall, P. & Delaney, P. T. 1982. Formation and interpretation of dilatant echelon cracks. Bull. geol, Soc. Am. 93, 1291-1303.

Rapin, W., et al., 2016. Hydration state of calcium sulfates in Gale crater, Mars: iden- tification of bassanite veins. Earth Planet. Sci. Lett. 452, 197–205. doi:10.1016/j. epsl.2016.07.045.

Ramsay, J. G. 1980. The crack-seal mechanism of rock deformation. Nature 284, 135–9

Ramsay, J. G. & Huber. M. I. 1983. The Techniques of Modern Structural Geology, Volume 1, Basic Techniques--Strain Analysis. Academic Press, London.

Rickard, M. J. & Rixon, L. K. 1983. Stress configurations in conjugate quartz-vein arrays. J. Struct. Geol. 5,573-578.

Rubin, D.M., et al., 2017. Fluidized-sediment pipes in Gale crater, Mars, and possible Earth analogs. Geology 45, 7–10. https://doi.org/10.1130/G38339.1

Schwenzer, S.P., et al., 2016. Fluids during diagenesis and sulfate vein formation in sediments at Gale crater, Mars. Meteorit. Planet. Sci. 28. doi:10.1111/maps. 12668.

Siebach, K.L., Grotzinger, J.P., Kah, L.C., Stack, K.M., Malin, M., Léveillé, R., Sum- ner, D.Y., 2014. Subaqueous shrinkage cracks in the Sheepbed mudstone: im- plications for early fluid diagenesis, Gale crater, Mars. J. Geophys. Res. Planets 119 (7), 1597–1613. doi:10.1002/2014JE004623.

Simms, M. J. and Rufell, A. H. 1990. Climatic and biotic change in the late Triassic. Journal of the Geological Society, London 147, 321–7

Stack, K.M., et al., 2014. Diagenetic origin of nodules in the Sheepbed member, Yellowknife Bay formation, Gale crater, Mars. J. Geophys. Res. Planets 119 (7), 1637– 1664. doi:10.1002/2014JE004617.

Stack, K. M., et al., 2015. Sedimentology and stratigraphy of the Pahrump Hills outcrop, lower Mount Sharp, Gale Crater, Mars, 46 calcium sulfate veins as observed by the ChemCam instrument, 46 Planetary Science Conference, 2 pp.

Stack, K. M., et al. 2016. Comparing orbiter and rover image-based mapping of an ancient sedimentary environment, Aeolis Palus, Gale crater, Mars, Icarus, doi:10.1016/j.icarus.2016.02.024.

Thomson, B.J., et al., 2011. Constraints on the origin and evolution of the layered mound in Gale crater, Mars using Mars Reconnaissance Orbiter data. Icarus 214 (2), 413–432. doi:10.1016/j.icarus.2011.05.002

Treiman, A.H., et al., 2016. Mineralogy, provenance, and diagenesis of a potassic basaltic sandstone on Mars: CheMin X-ray diffraction of the Windjana sam- ple (Kimberley area, Gale crater). J. Geophys. Res. Planets 121 (1), 75–106. doi:10.1002/2015JE004932.

Ukar, E., Lopez, R.G., Laubach, S.E., Gale, J.F.W., Manceda, R., Marrett R., 2017. Microfractures in bed-parallel veins (beef) as predictors of vertical macrofractures in shale: Vaca Muerta Formation, Agrio Fold-and-Thrust Belt, Argentina, Journal of South American Earth Sciences, 79, pp. 152-169, 10.1016/j.jsames.2017.07.015

Vaniman, D.T., et al., 2018. Gypsum, bassanite, and anhydrite at Gale crater, Mars. Am. Mineral. 103, 1011–1020. https://doi.org/10.2138/am-2018-6346

Villanueva G. L. et al., 2015. Strong water isotopic anomalies in the Martian atmosphere: Probing current and ancient reservoirs. Science 348:218–221.

Wagner, R. V., Henriksen, M.R., Manheim, M.R., Robinson, M.S., 2014. Photoscan for Planetary and Analogues Sites, in: 3rd Planetary Data Workshop. p. 7023. https://doi.org/10.1016/j.icarus.2014.04.002

Watkins, J. A., et al., 2017. Fracture formation by compaction-related burial in Gale crater, Mars: implications for the origin of Aeolis Mons, Lunar Plan. Sci. Conference, pp 3019

Whittaker, A. and Green, G. W. 1983. Geology of the country around Weston-super-Mare, memoir for 1:50,000 geological sheet 279. New series, with parts of sheet 263 and 295. Geological Survey of Great Britain, Institute of Geological Sciences. London: Her Majesty's Stationery Office, 147 pp.

Wiens, R. C. and 80 co-authors, 2012. The ChemCam instrument suite on the Mars Science Laboratory (MSL) rover: body unit and combined systems, Space Sci. Rev., 170 :167-227, doi 10.1007/s11214-012-9902-4.

Wray, J. J., 2012. Gale crater: The Mars Science Laboratory/Curiosity Rover Landing Site, Int. J. Astrobiol., doi:10.1017/S1473550412000328.

Young, B.W., Chan, M.A., 2017. Gypsum veins in Triassic Moenkopi mudrocks of southern Utah: Analogs to calcium sulfate veins on Mars. J. Geophys. Res. 150–171. https://doi.org/10.1002/2016JE005118

Figure 1. In panel (a) the yellow line with stops displays the Curiosity rover traverse; in the red circle the study area is highlighted; the blue dashed line represents the contact between the Bradbury group (NW) and the Mount Sharp group (SE). (b) Gale crater surveyed region. (c) Stratigraphic column of Gale crater sedimentary rocks (modified after Hurowitz et al., 2017).

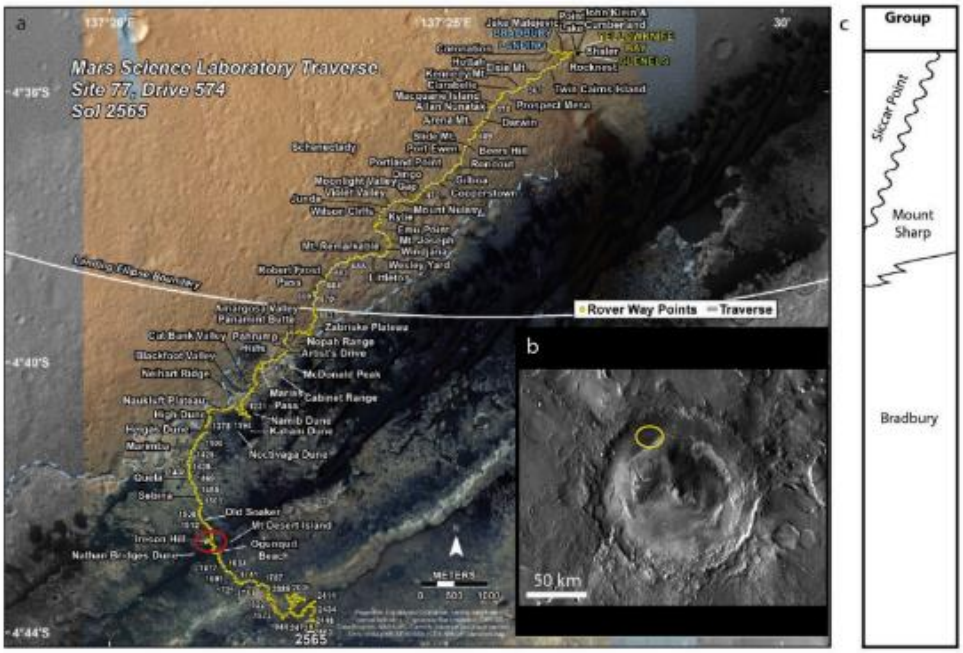

Figure 2. (a) 3D Digital Outcrop Model (DOM) of the region of interest within the area that Curiosity rover observed between sol 1536 and 1545. (b) Computation output and histogram of the point cloud volume density (green portions display maximum density values). (c) Magnification of a portion of the study area. Plains are displayed on the texture and the dense point cloud.

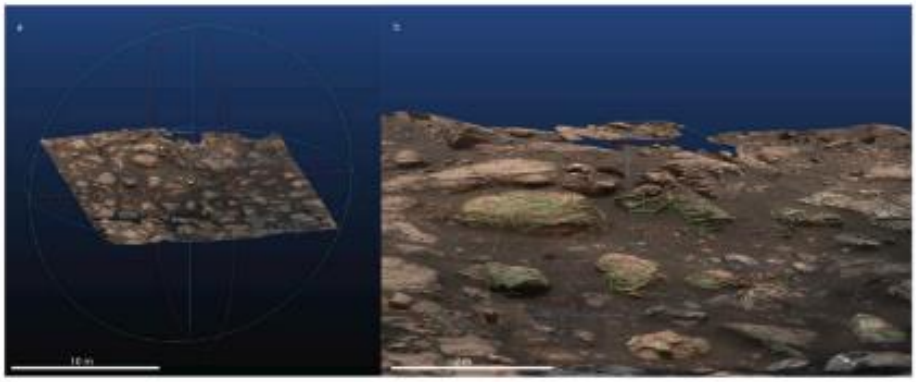

Figure 3. Stitched landscape of the main outcrop within the area of interest. The three different identified sets are highlighted below. (a) oblique set of veins where “en-echelon” structures have been recorded and preserved; (b) horizontal set, veins following the crosscutting lamination trend are highlighted; (c) conjugate oblique vein set where the crosscutting relationship between sets is well visible.

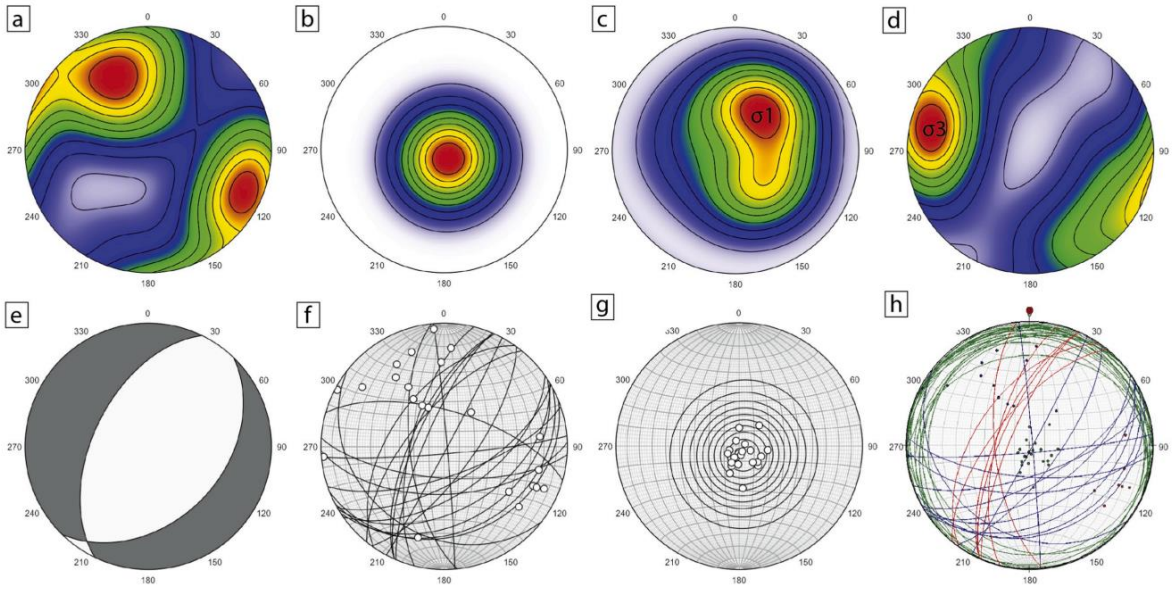

Figure 4. The stereo plots show: the orientation of the oblique (a,f) and bedding-parallel (b,g) fracture planes detected on the study area on Mars; the maximum and minimum stress orientations (c,d) and the kinematics extracted from the oblique vein set's data (e). Dataset extracted from the 3D DOM: 46 planes.